Novel Correlation Approach Between Actual Air Properties of Isothermal Process Used in Compressed Air Energy Storage

Mohamed Ammar¹, Changzhao Jiang², Nikos Dimolios³, Vagelis Ikonomou⁴, Muhammad Imran Khan⁵

^{1, 2} Department of Mechanical and Aerospace Engineering, Brunel University London, Uxbridge, United Kingdom

³ Nikolaos Dimolios is the CTO of Metapower, United Kingdom

Abstract:- This study introduces novel correlation models for compressed air energy storage, which incorporate the authentic features between the Actual Air (AA) properties used. Furthermore, these proposed models examine the thermodynamic characteristics employed in Isothermal processes. This paper additionally provides a comprehensive coverage of both theoretical understanding and practical implementation of the idea. The found correlations aid in the understanding of the core thermodynamic principles related to compressed air energy storage (CAES). The primary objective of this study is to comprehensively understand the characteristics and attributes of Actual Air (AA) through the establishment of a theoretical framework. Furthermore, it underscores the significance of precise fluid property data in the computation and development of Compressed Air Energy Storage (CAES) systems. This study aims to investigate the hypothesised correlations between the physicochemical characteristics of air and the assessment of cycle efficiency in the Isothermal process.

Keywords: Energy Storage, Energy Systems, Actual Air Properties, Compressed Air Energy Storage, I-CAE.

1. Introduction

Initially, the hydro-pneumatic energy storage system implemented the concept of isothermal compressed air energy storage (I-CAES). The gas is compressed by means of a liquid in these devices. In the context of Closed-cycle Hydro-Pneumatic Energy Storage (C-HyPES), the process involves the injection of a liquid into the storage tank, resulting in a reduction of gas volume and subsequently an elevation in gas pressure as shown in **Figure 2**. In order to meet the need for energy, the gas pressure is decreased by enabling the liquid to pass through the pump turbine (P/T) in a reverse direction. In this configuration, the pump turbine operates as a turbine, driving the generator [1]–[3]. One of the primary concerns associated with C-HyPES is its low energy density. As a result, the absence of commercial iterations of these systems is evident, although ongoing laboratory-scale experimentation is being conducted [3]–[5]. In order to address the limitations associated with C-HyPES, the O-HyPES idea has been developed, which integrates the enhanced energy densities of air-air systems with the benefits of utilising a liquid as the working medium. In an O-HyPES (Ocean Hybrid Power and Energy Storage) system, the process involves the compression of air using a liquid piston prior to its entry into the Compressed Air Storage (CAS) at elevated pressure, as shown in **Figure 2**.

This particular concept necessitates the presence of a minimum of two alternate cylinders, which can facilitate the pumping of a liquid in and out. Additionally, a system of valves is required to enable a cyclic air supply and release [3], [4], [6], [7]. The O-HyPES technology, in contrast to the closed cycle system, has demonstrated

⁴ Department of Mechanical and Aerospace Engineering, Imperial College London, United Kingdom

⁵ Department of Mechanical Engineering, Prince Mohammad Bin Fahd University, Al-Khobar, Saudi Arabia

successful implementation at the laboratory scale [8]-[10]. Furthermore, it has experienced further advancements to enable its utilisation as a utility-scale storage unit. The initial pilot plant, boasting a power capacity of 2 MW, was constructed in Texas and has undergone testing since 2012 [11]-[14]. The power exchange during both the charging and discharging processes is limited due to the heat exchange surface formed by the contact between the liquid and gas phases. The efficiency of the process, which is no longer isothermal, exhibits a decline with higher power levels due to the observed increase in temperature gradients. One potential method for addressing this limitation is to introduce water into the compression chamber, creating a significant water surface area that interacts with the gas [15]-[18]. This methodology facilitates the utilisation of traditional piston technology through the attainment of an effective heat transfer mechanism. In order to effectively tolerate the presence of water content, appropriate modifications must be made to the accompanying piston compressors/expanders. The latest finding of this study, as stated in reference [19], [20], pertains to the compression of pre-mixed foam as a means to enhance heat transmission. In order to lessen the amount of thermal energy wasted, a considerable number of studies into novel approaches have focused on compressed air energy storage (CAES) devices. Recent research by the authors of [21]-[24] suggests that by using an original design for the compressor and expander, isothermal compressed air energy storage (I-CAES) cycles can be realised as shown in Figure 1 [25]-[27], this structure makes it much easier to remove heat from the air during compression and then add it back in during expansion.

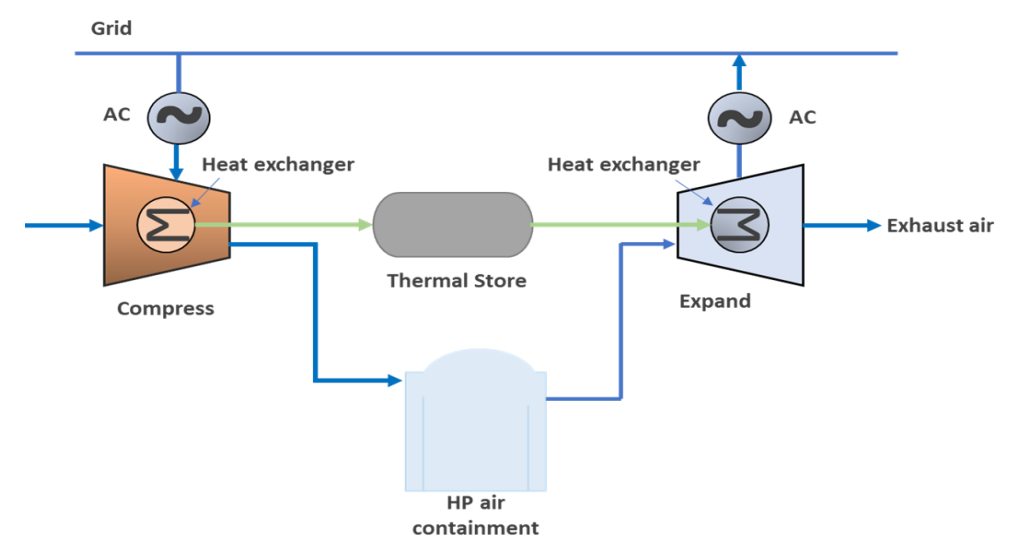


Figure 1. Schematic diagram of I-CAES.

2. Closed-cycle Hydro-Pneumatic Energy Storage (C-HyPES),

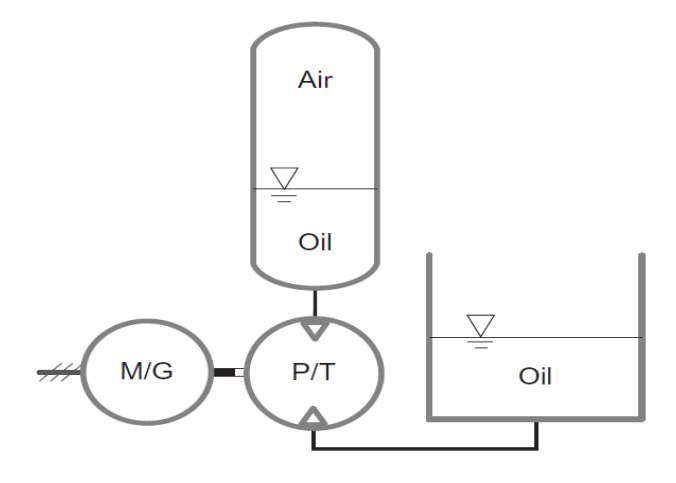


Figure 2. Schematic diagram of I-CAES C-HyPES

C-HyPES consists of two stage modes, which are the charging and discharging modes. These procedures will be performed through the PAT (Pump as Turbine). In this section, the entire system will be viewed as a couple of the tanks been connected through the pipe, where one of them will be treated as the liquid inside the C-HyPES, while the other will be treated as the outer tank. The type of the flowing mode (charging and discharging modes) would governs the locations of the tanks as well as the direction of the flow between them. Various methods have been employed in compressed air energy storage (CAES) systems to enhance heat transfer, such as the utilisation of liquid droplets, liquid piston air compressors/expanders, porous inserts, and hollow spheres. These methodologies have demonstrated efficacy. The construction of a perfect isothermal plant is highly improbable due to the heat generated by gases during compression and the limited compressibility of liquids. Despite the existence of several proposed alternatives, the realisation of such a plant remains doubtful. In the year 2013, a study conducted by [28], [29]involved the development of a prototype for a 1.5 MW I-CAES system. During the compression phase, heat absorption was achieved by spraying water onto the piston. In previous studies, scholars [30]–[35]have successfully devised a liquid piston that emulates the configuration of reciprocating mechanisms, aiming to enhance the reversibility of gas compression and expansion. This methodology does not examine studies that employed conventional volumetric expanders for achieving isothermal or quasi-isothermal compression and expansion [11], [36]–[40]. The given design of the liquid piston aims to optimise the surface area to volume ratio, minimise heat loss, and achieve nearly isothermal operation within a gas chamber. The desired outcome can be attained through the manipulation of gas within a chamber of fixed capacity, employing either compression or expansion techniques, and incorporating a liquid column [41]-[44].

To enhance the isothermal performance of compressed air energy storage (CAES), the implementation of drop spray injection heat transfer was incorporated alongside the liquid piston mechanism. The purpose of this action was to enhance the system's efficiency. The user did not provide any text to rewrite. This endeavour was undertaken with the intention of achieving the predetermined objectives. The integration of this method has been observed to be efficacious in mitigating the air temperature and maintaining operational conditions in close proximity to isothermal levels (76). The initial technology for wind turbines known as isothermal compressed air energy storage (I-CAES) was developed by [45], [46]. This innovative approach incorporates liquid pistons and employs isothermal refrigeration techniques. Furthermore, the authors in reference [78] employed a liquid pistonbased isothermal compressed air energy storage (I-CAES) system to carry out empirical investigations on porous inserts. The apparatus utilised in the research has a compression-to-expansion ratio of 10:6. Furthermore, the utilisation of a liquid piston in conjunction with the incorporation of a water spray or droplet has the potential to enhance heat transfer. This alternative can be implemented as a substitute for the liquid piston. [47]–[49] have developed an isothermal compressed air energy storage (I-CAES) system that exhibits rapid heat absorption and emission capabilities throughout its charge and discharge processes. This approach utilises reciprocating equipment to administer a concentrated mist spray. Previous studies have been conducted on reciprocating machines, as well as other mechanical devices such as screws and scrolls [48], [50]–[53].

The research conducted by [82] encompassed the examination and development of a pumped hydro compressed air energy storage system (PH-CAES). The findings of the experiment indicated that the PH-CAES system demonstrated the capability to function at almost isothermal conditions. The polytrophic exponent of air was determined to be 1.07 for power generation and 1.03 for energy storage. The values in question were discovered as a result of rigorous research. Furthermore, the performance of the PH-CAES system exhibited a roundtrip efficiency of 51%. Furthermore, the collective efficiencies of the many components within the system play a crucial role in determining the total round-trip efficiency of the system. For example, PH-CAES exhibits an efficiency of 63 percent, even when the hydro turbine producing units are operating at a high efficiency level of 90 percent. The utilisation of this approach in commercial applications is currently limited due to the inherent challenges associated with its empirical validation [54]–[56]. There has been a proposal to utilise isothermal or near-isothermal systems for the purpose of storing energy in compressed air and releasing energy from expanded air, as mentioned in reference [57], [58]. The objective of this advice is to enhance the round-trip efficiency of the CAES system while simultaneously reducing the associated costs. These strategies would entail the storage of energy by compressing air while ensuring temperature stability.

3. Novel Correlation Approach

3.1. Closed-cycle Hydro-Pneumatic Energy Storage (C-HyPES)

3.1.1. Charging Mode Process

During the charging process, the centrifugal pump will function in pump mode, whereby the fluid in motion will be propelled vertically upwards, as seen in Figure 3.

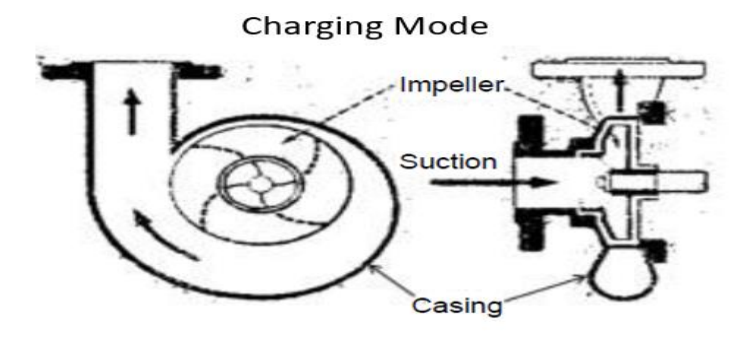


Figure 3. Charging mode of the centrifugal pump.

Head Loss Equation: Figure 4 depicts the schematic diagram representing the pair of tanks that were subjected to the ambient environment. The flow mode of this system may be conceptualised as the transfer of fluid from the lower tank to the upper tank. In order to facilitate this process, the system requires the use of a pump. It is assumed that each surface of the liquid exposed inside the tanks is subjected to a specified external pressure.

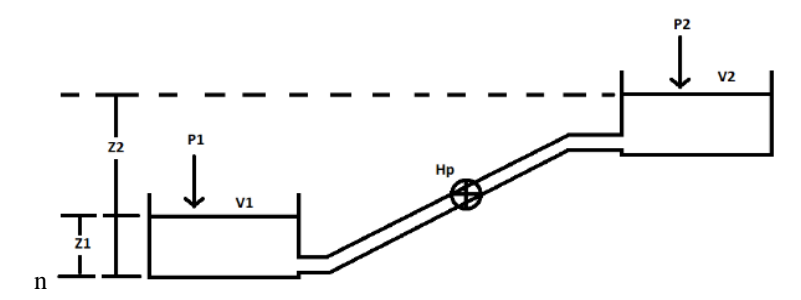


Figure 4. Shows the schematic diagram of tanks connected with a pump

In accordance with the Bernoulli principle, the following is a description of the connection that exists between the several shown parameters that are shown in **Figure 4.**

$$\left(\frac{P_1}{\rho g} + \frac{v_1^2}{2g} + z_1\right) - \left(\frac{P_2}{\rho g} + \frac{v_2^2}{2g} + z_2\right) = -H_p$$
(1)

Where

 P_1 = External Pressure acting on the liquid's surface within the lower tank.

 P_2 = External Pressure acting on the liquid's surface within the higher tank.

 v_1 = Speed of the liquid's surface within the lower tank.

 v_2 = Speed of the liquid's surface within the higher tank.

 z_1 = Elevation of the liquid's surface within the lower tank.

 z_2 = Elevation of the liquid's surface within the higher tank.

 H_p = Hydraulic Power been gained by the Pump.

Tuijin Jishu/Journal of Propulsion Technology

ISSN: 1001-4055 Vol. 44 No. 6 (2023)

The link between the velocities at both tanks is shown in Eq 2 based on the principle of continuity for an incompressible fluid.

$$Q = A_1 v_1 = A_2 v_2 (2)$$

Therefore, through the involvement of the continuity, the entire expression of the Bernoulli Equation can be defined in terms of the flow-rates, which is given below:

$$\left(\frac{P_1 - P_2}{\rho g}\right) + \left(z_1 - z_2\right) + \frac{Q^2}{2g} \left(\frac{1}{A_1^2} - \frac{1}{A_2^2}\right) = -H_p$$
(3)

Pump's Head Equation: The head of the Pump for a given flow-rate is defined as the follows:

$$\frac{H_p}{H_{p_{P(BEP)}}} = 1.245 - \left(\frac{Q}{Q_{P(BEP)}}\right)^2$$
 (4)

Where $H_{p_{BEP}}$ and Q_{BEP} denote for the head of the pump and the flow-rate at the best efficiency point, the point where the efficiency for given pump would perform at its maximum value.

3.1.2. Pump's Efficiency Equation

The efficiency of a given Pump is defined as the following:

$$\eta_{p} = \frac{\left(A + BH_{p} + CQH_{p} + DQ^{2}H_{p} + EH_{p}^{2} + EH_{p}^{2} + FQH_{p}^{2} + GQ^{2}H_{p}^{2}\right)}{100}$$
(5)

Where

$$A = 80$$
 $B = -0.9367$ $C = 5.46 \times 10^{-3}$ $D = -1.514 \times 10^{-5}$ $E = 5.802 \times 10^{-3}$ $F = 3.028 \times 10^{-5}$ $G = 8.346 \times 10^{-8}$

Input Pump's Power Equation: Input Power is determined from the following expression:

$$P_{P} = \frac{\rho g Q H_{P}}{\eta_{P}} \tag{6}$$

Dimensionless Numbers: The following expressions display some of the dimensionless numbers that were used for the analysis of the flow throughout the charging mode within the centrifugal pump.

$$\psi = \frac{gH_p}{n^2D^2} \tag{7}$$

$$\phi = \frac{Q}{(nD^3)} \tag{8}$$

Assuming that the dimensions (D) and the speed (n) within PAT is similar to that been used by [59]; by employing the concept of the dimensional similarity, the operated flow-rate and the pump's head throughout the pump will be same as that been used by [59].

Therefore the expressions for the Head in Eq 4 and Efficiency in Eq 5 for the pump would still be same as that been proposed by [59].

3.1.3. Discharging Process

Throughout the discharging process, the centrifugal pump will be operated as a discharging mode, where the flowing fluid will be pumped pump run in reverse as it illustrated in **Figure 5**.

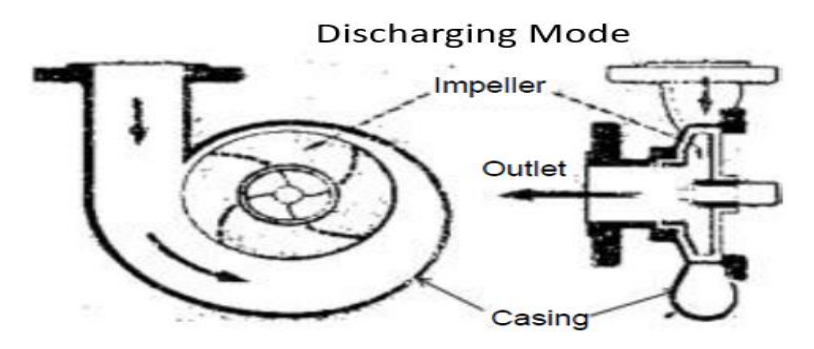


Figure 5. Discharging Mode of the centrifugal Pump.

Head Loss Equation: A diagram illustrates for the flowing fluid that takes place between the tanks, where the turbine is positioned between them.

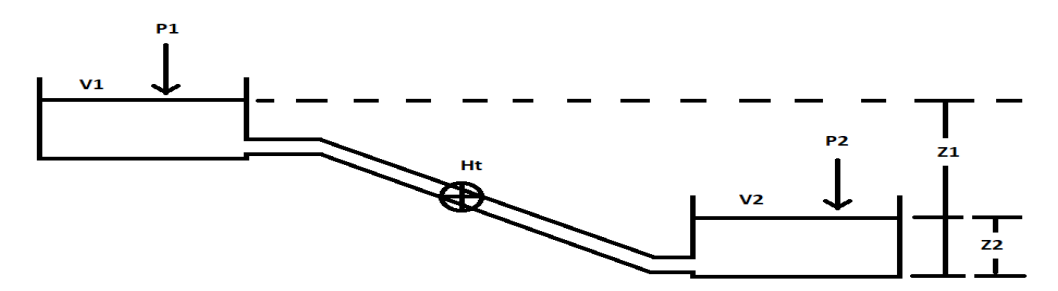


Figure 6. Shows the schematic diagram of tanks connected with a turbine.

Principle of Bernoulli for the above-mentioned diagram is shown as the following, where the fluid would have lost some energy due to the turbine:

$$\left(\frac{P_1}{\rho g} + \frac{v_1^2}{2g} + Z_1\right) - \left(\frac{P_2}{\rho g} + \frac{v_2^2}{2g} + Z_2\right) = H_t$$
(9)

 H_t = Head lost by the turbine.

Turbine's Head: The head of the turbine for a given flow-rate is defined as follows:

$$\frac{H_T}{H_{T(BEP)}} = 1.0283 \left(\frac{Q}{Q_{T(BEP)}}\right)^2 - 0.5468 \left(\frac{Q}{Q_{T(BEP)}}\right) + 0.5314$$
(10)

For the **Eq 10**, both of Head $H_{T(BEP)}$ and Flow-rate $Q_{T(BEP)}$ at the best Efficiency Point were obtained using the following expressions:

$$H_{T(BEP)} = H_{p(BEP)} \left(\frac{1}{\eta_p^{1.2}} \right) \tag{11}$$

$$Q_{T(BEP)} = Q_{p(BEP)} \left(\frac{1}{\eta_p^{0.8}} \right)$$
 (12)

Where η_p denotes the maximum efficiency been performed by the Pump.

Turbine's Output power: The Output Power of the turbine was obtained using the following expression:

$$P_{T(BEP)} = \eta_{T(BEP)} \rho_g Q_{T(BEP)} H_{T(BEP)}$$
(13)

Where it is assumed that the efficiency of the Turbine at the best Efficiency Point would be taken to be same as that of the Pump as proposed by Sharma [].

$$\eta_{T(BEP)} = \eta_{P(BEP)} \tag{14}$$

The output power of the turbine for a given flow-rate is defined as follows:

$$\frac{P_T}{P_{T(BEP)}} = -0.3092 \left(\frac{Q}{Q_{T(BEP)}}\right)^3 + 2.1472 \left(\frac{Q}{Q_{T(BEP)}}\right)^2 + 0.8865 \left(\frac{Q}{Q_{T(BEP)}}\right) + 0.0452$$
(15)

The efficiency of the turbine is determined from the following expression:

$$\eta_T = \frac{\rho g Q H_T}{P_T} \tag{16}$$

3.2. Ocean Hybrid Power and Energy Storage (O-HyPES)

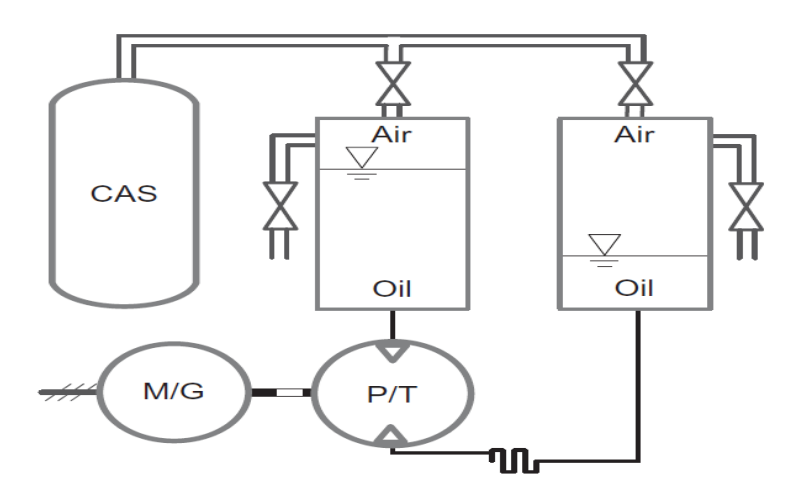


Figure 7. Schematic diagram of I-CAES O-HyPES

In this section, the behaviour of this system would simply divide into four stages, which is shown as follows:

Stage 1: When both of the left and right valves into the Compressed Air Storage are closed and the Pump is been operating through this stage. This stage has used **Eqs 1-5.**

Stage 2: When the left valve into the Compressed Air Storage is open and the right valve is closed, while the Pump is still operating. This stage has used **Eqs 1-5**.

Stage 3: When both of the left and right valves into the Compressed Air Storage are closed and the Turbine is been operating through this stage. This stage has used **Eqs 8-16**.

Stage 4: When the left valve is closed and the right valve is into the Compressed Air Storage is open, while the Turbine is still operating. This stage has used **Eqs 8-16.**

4. Results and Analysis for C-HyPES

4.1. Selected Variables for the C-HyPES

The following table illustrate the conditions that were used throughout the charging and discharging modes within the C-HyPES.

Table 1. Shows the conditions used for charging and discharging modes in the C-HyPES.

Operating Conditions	
Temperature of air within C-HyPES / °C	20
Pressure of air within C-HyPES / atms	1
Mass of the stored air within C-HyPES / kg	0.2
Maximum Volume of the stored air within C-HyPES (from the datum) / m ³	0.2
Maximum Height of the stored air within C-HyPES (from the datum) / m	0.67
Temperature of air at the outer tank / °C	20
Pressure of air at the outer tank / atms	1
Density of the Liquid / (kg/m³)	700
Flow-rate through Pump at (BEP) / ((m ³)/h)	300
Head through Pump at (BEP) / (m)	50
Maximum Pump's efficiency	0.8
Maximum Turbine's efficiency	0.8
Cross-sectional Area of C-HyPES / m ²	0.3
Cross-sectional Area of outer tank / m ²	0.5

4.2. Resulted Variables of Charging Process

Pressure; Plot 1 seen in **Figure 8** demonstrates the temporal fluctuation of Air Pressure. Based on the data shown in the aforementioned table, it is evident that the air pressure exhibits a gradual rise over time. However, it is noteworthy that the duration required for the pressure to reach a state of equilibrium is around 0.7 seconds.

Height of liquids' surfaces; The plot 2 shown in Figure 8 illustrates the change of the liquid's surface in both tanks when the air is compressed in relation to the datum. The rise in the height of the liquid's surface inside C-HyPES may be attributed to the compression exerted on the liquid by the pump during the charging mode. Conversely, the reduction in the liquid's surface level in the outer tank over time may be attributed to the incompressible nature of the fluid used throughout the procedure.

Flow-rate; Plot 3 in **Figure 8**, illustrates the temporal changes in flow-rate throughout the compression process. There is an observed trend of decreased flow-rate over time. This phenomenon may be linked to the decrease in the pressure differential between the surfaces of the liquids and their disparity in height.

Velocity of Liquids' Surfaces; Plot 4 in **Figure 8** shows the decrease in flow rate over time led to a corresponding decrease in the velocities at the surfaces of the liquids in both the C-HyPES and outside tank.

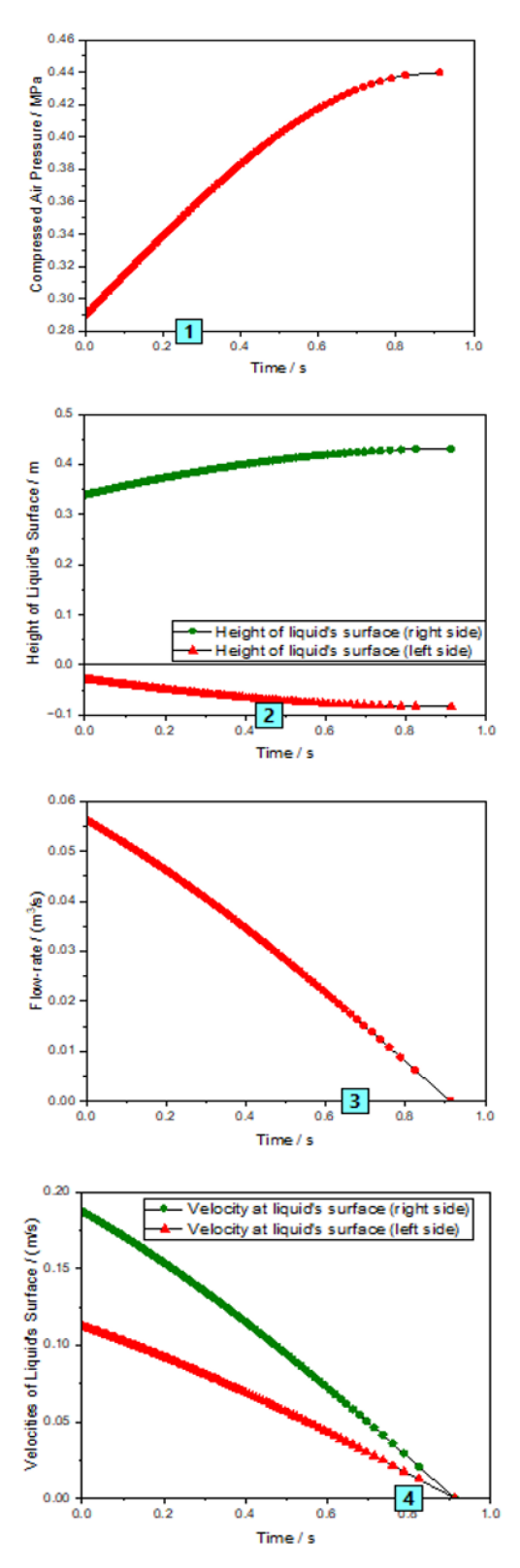
Pump's Head; Plot 5 in **Figure 8** depicts the fluctuation of the Pump's Head during the duration of the charging mode procedure. In line with the aforementioned discussion on pressure, it is seen that the head of the pump exhibits an increasing trend over time. Nevertheless, it is noteworthy that the duration required for the head to reach a state of equilibrium, where no more alterations occur, is around 0.7 seconds.

Pump's Efficiency; Plot 6 in **Figure 8** illustrates the temporal fluctuation of the efficiency of the pump during the compression process. There is an observed trend of decreased flow rate over time. The decrease in flow rate over time during the charging mode is believed to be caused by the dependence of the pump's efficiency on both the flow rate and the pump's head.

Pump's Input power; Plot 7 in Figure 8 illustrates the temporal fluctuations in the input power of the Pump. The observed trend indicates that the input power of the pump gradually rises until reaching its maximum at 0.2 seconds. This may be attributed to the dominance of the pump's head growth rate over the decline in flow rate, as

Vol. 44 No. 6 (2023)

well as the influence of the pump's efficiency. When the duration exceeds 0.2 seconds, it has been observed that the input power of the pump reduces. This reduction is believed to be caused by the combined influence of the lowering flow rate and the pump's efficiency, which outweighs the impact of the growing pump head on the pump's power.



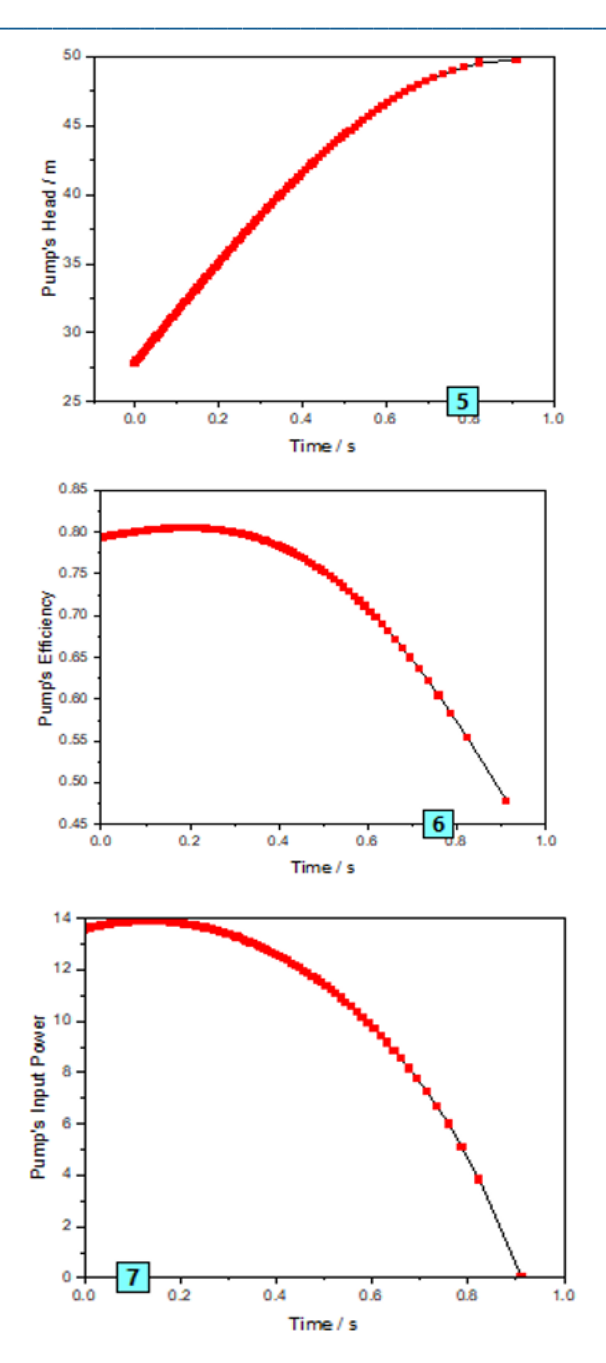


Figure 8. Shows 7 plots Resulted Variables of Charging Process

4.3. Resulted Variables of Discharging Process

Pressure; Plot 1, **Figure 10** depicts the temporal changes in Air Pressure during the discharging operation. It has been found that the air pressure gradually drops over time inside the C-HyPES system, eventually stabilising at around 3.07 atmospheres after approximately 5.5 seconds. At this point, the air pressure within the C-HyPES system ceases to change further.

Height of liquids' surfaces; Plot 2, **Figure 10** illustrates the alteration of the liquid's surface in both tanks during the discharge mode in the C-HyPES system, relative to the reference point. As previously discussed in the Charging mode section, it is important to note that the fluid used in this system is considered incompressible. Consequently, any increase non the volume of liquid inside the outer tank will correspond to an equivalent decrease in the volume of liquid within the C-HyPES.

Flow-rate; The plot under consideration is Plot 3. The flow-rate fluctuation during the discharging mode with respect to time is shown in **Figure 10**. As previously discussed in the charging section, the decrease in flow rates may be attributed only to the decrease in the pressure difference between the surfaces of the liquids and the decrease in their height difference.

Velocity at liquids' Surfaces; Plot 4 in **Figure 10** illustrates the changes in the surface velocities of the liquids inside both tanks throughout the discharging mode. As previously stated in the charging mode section, the decrease in flow rates resulted in a corresponding decrease in velocities at the surfaces of the liquids in both the C-HyPES and outside tank, as seen in the accompanying graph.

Turbine's Head; Plot 5, **Figure 10**, illustrates the temporal variation of the Turbine's Head in the discharge mode. It has been observed that the turbine's elevation is gradually lowering over time until it hits a minimal value at around 0.75 seconds. Subsequently, the elevation of the head pump starts, with a gradual reduction in its gradient seen over time.

Turbine's Output power; Plot 6 Figure 10 illustrates the temporal fluctuations in the output power of the turbine. The power derived using equation (48) demonstrates notable accuracy for time intervals less than about 0.25 seconds and larger than 2.6 seconds. It is suggested that this equation is particularly suitable for lower flow rates through the turbine. It has been observed that there is a discernible rise in the power output of the turbine beyond a time interval of 2.6 seconds. This phenomenon may be attributed to the dominance of the turbine's head, which supersedes the influence of flow rates on the power production during this specific period.

Turbine's Efficiency; Plot 7, **Figure 10** displays which represents the fluctuation of the Turbine's Efficiency in the discharging mode over time. The increase in turbine efficiency, similar to the reasons mentioned for the Head's Pump, has been observed for a duration exceeding 2.6 seconds. This suggests that the impact of the turbine's head is more significant than the influence of flow rates on the output power during this time period.

4.4. Head's Pump Impact Overall Cycle Efficiency at Best Efficiency Point (BEP)

Figure 9 depicts the relationship between the Overall Cycle Efficiency and the pump's Best Efficiency Point (BEP) for various Pump Efficiencies. It has been observed that there is a positive correlation between the head's pump (BEP) and the Overall Cycle Efficiency, indicating that an increase in BEP generally leads to an improvement in efficiency. It has been observed that the values of the Overall Cycle Efficiency are higher when the Pump's Efficiency is 0.85 compared to when it is 0.8.

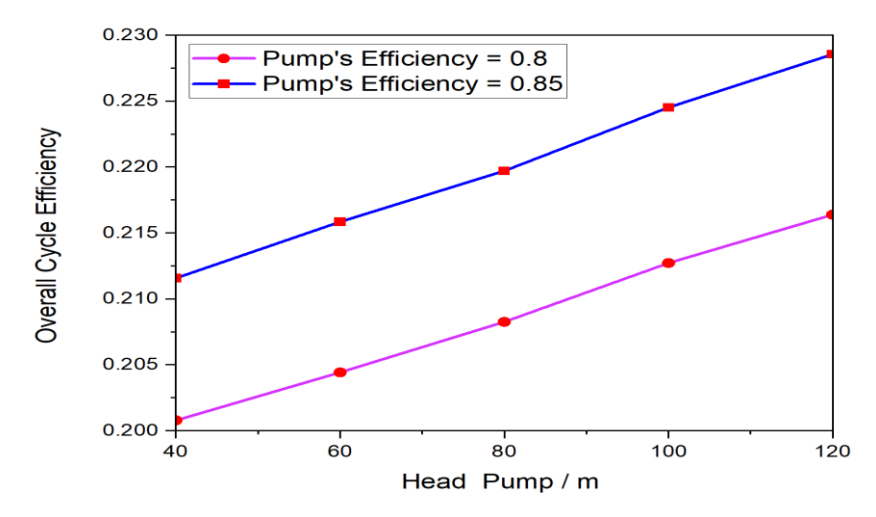
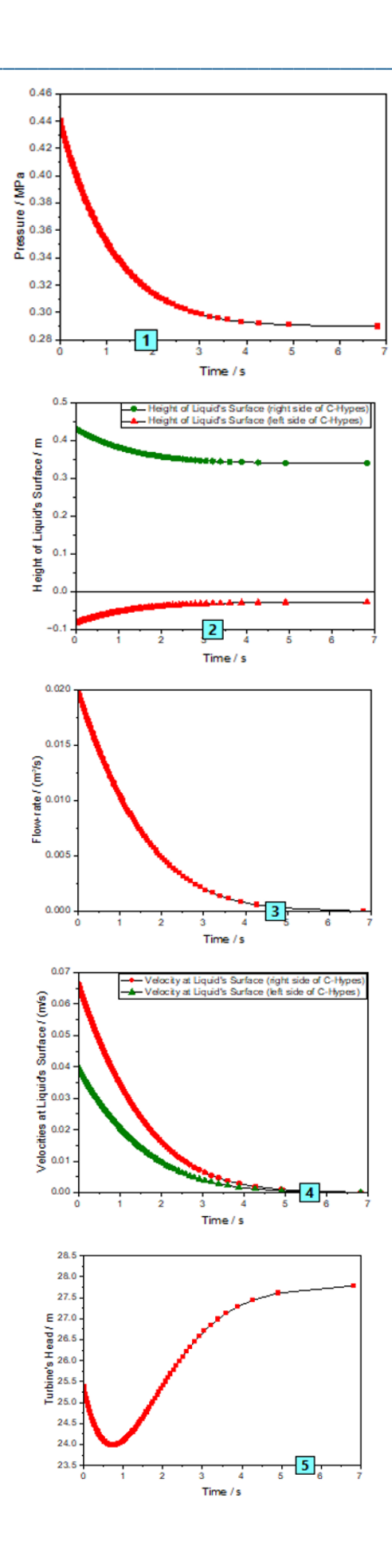


Figure 9. Overall Cycle Efficiency vs Pump's Head (BEP) for different Efficiencies.



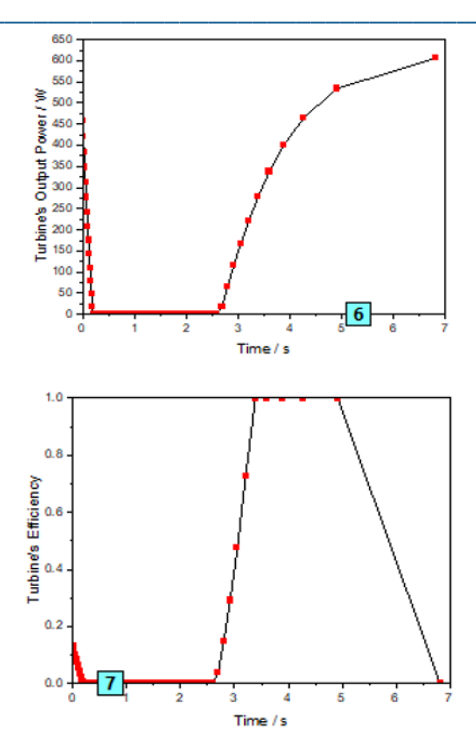


Figure 10. Shows 7 Plots of the Resulted Variables of Discharging Process

5. Results and Analysis for O-Hypes

5.1. Selected Variables throughout the process

Table 2. Shows the conditions used for charging and discharging modes in the O-HyPES.

Operating Conditions	
Temperature of air within each of the cylinders throughout the process / °C	20
Initial mass of the stored air within each of left and right cylinders / kg	1.5
Maximum Volume of the stored air within O-HyPES (from the datum) $/\ m^3$	0.9
Maximum Height of the stored air within O-HyPES (from the datum) $/$ m	1.5
Density of the Liquid / (kg/m³)	700
Flow-rate through Pump at (BEP) $/$ ((m ³)/h)	140.58
Head through Pump at (BEP) / (m)	40
Maximum Pump's efficiency	0.8
Maximum Turbine's efficiency	0.8
Cross-sectional Area of each of left and right cylinders \slashm^2	0.6
Initial Pressure within the Compressed Air storage /	1
Volume of Compressed Air Storage (CAS) / m ³	0.6

5.2. Resulted Variables of Stage 1

Pressure; Plot 1, **Figure 11** depicts the temporal fluctuation of Air Pressure. Based on the data shown in the aforementioned table, it can be noticed that the air pressure experiences a rise over a time span of about 3.7 seconds, reaching a point beyond which no further increase is visible.

Height of liquids' Surfaces; Plot 2 **Figure 11** illustrates the changes in the liquid surface of each tank as a consequence of air compression relative to the reference point. The increase in the height of the liquid's surface

Vol. 44 No. 6 (2023)

inside the left cylinder over time may be attributed to the pump's compression of the liquid during charging mode, as explained in the C-HyPES section. Conversely, the decrease in the liquid's surface level on the right cylinder suggests that the experimental method used an incompressible fluid.

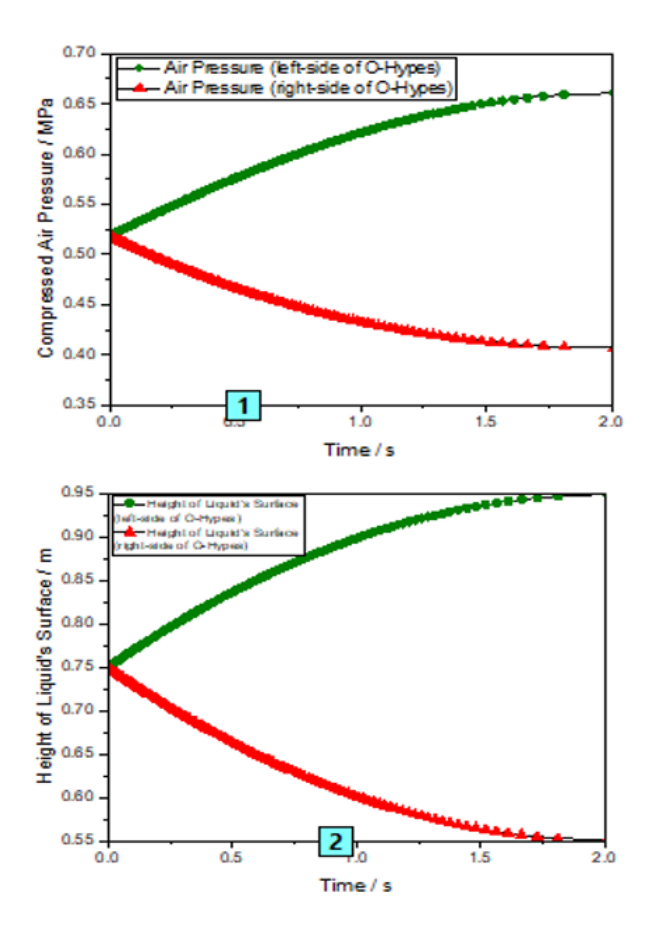
Flow-rate; Plot 3 **Figure 11** illustrates how the flow rate changed during the course of the compression in relation to the passing of time. It can be seen that the flow rate tends to decrease with time, which results in a lowering of the pressure difference between the surfaces of the liquids as well as their height difference.

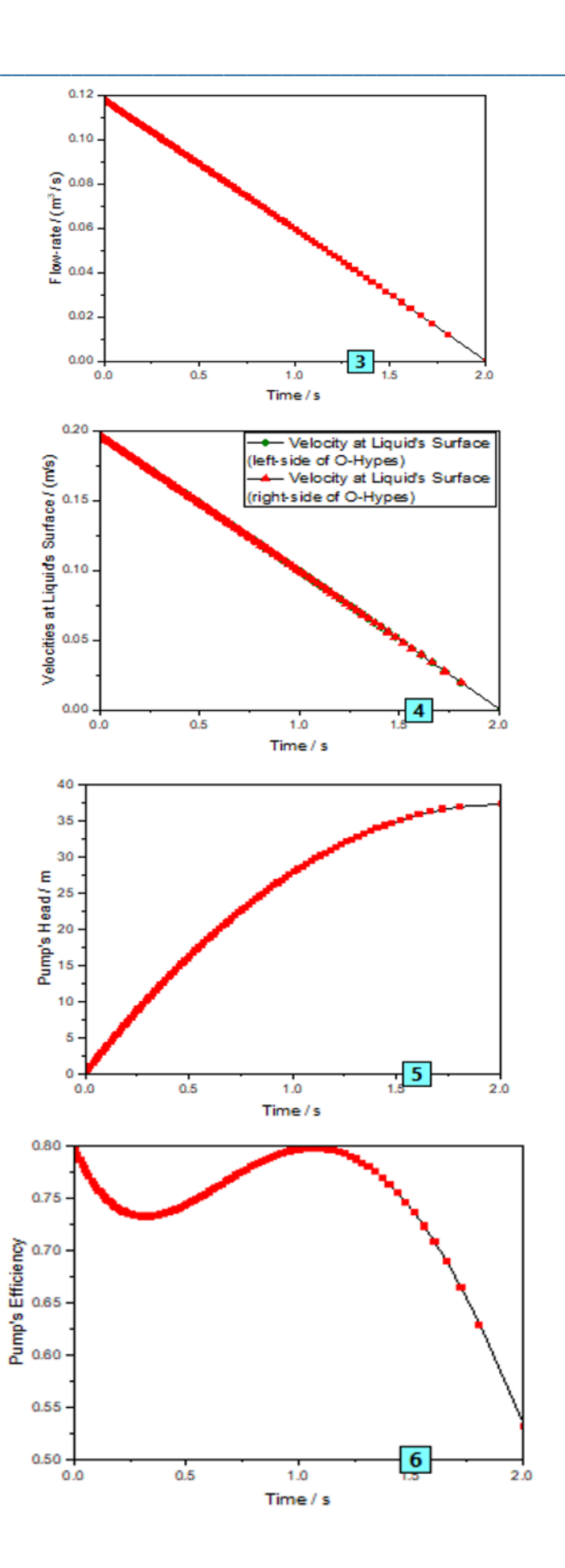
Velocity at liquids' Surfaces; Plot 4 Figure 11 shows the gradual drop in the flow rate over the course of time resulted in a slowing of the velocities at the liquids' surfaces inside O-HyPES, as the accompanying graph demonstrates.

Pump's Head; Plot 5 **Figure 11** illustrates how the Pump's Head has been changing over time while the charging mode operation has been going on. In a manner similar to that which has been described for the pressure, the head of the pump rises as the amount of time passes.

Pump's Efficiency; Plot 6 **Figure 11** illustrates the temporal fluctuation of the efficiency of the pump during the compression process. The key moment for the value of the pump's efficiency occurs at around 0.5 seconds, as a result of the combined effects of the falling flow rate and rising pump head over time. The efficiency then reached its peak value of 0.8 after about 2 seconds, after which it began to decline.

Pump's Input power; Plot 7 **Figure 11** depicts the temporal fluctuation of the input power of the Pump. The observed phenomenon indicates that the input power of the pump exhibits a growing trend till reaching its maximum value at 1.5 seconds. This behaviour is attributed to the dominance of the pump's head growth rate over the lowering flow-rate, as well as the efficiency of the pump. When the duration exceeds 1.5 seconds, it has been observed that the input power of the pump reduces. This decrease is believed to be caused by the reduction in flow rate, and the efficiency of the pump determines how the increase in pump head affects its power.





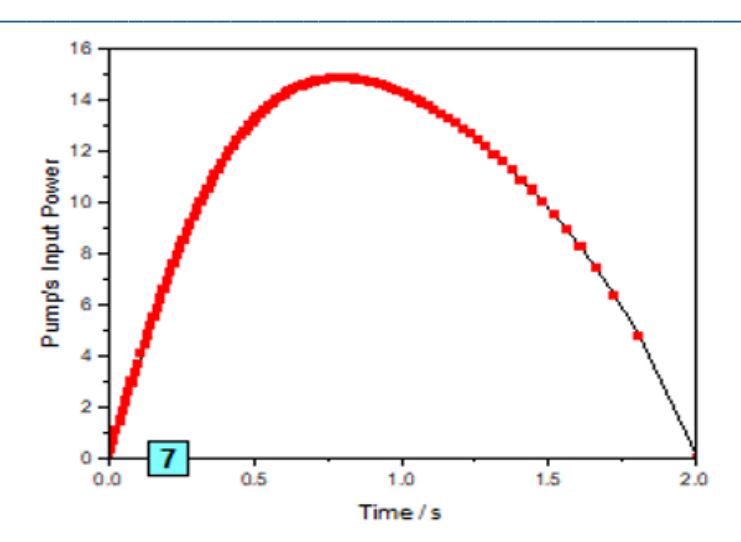


Figure 11. Shows 7 Plots of Resulted Variables of Stage-1 of O-HyPES

5.3. Resulted Variables of Stage 2

Pressure; Plot 1 in **Figure 12** is the graph that demonstrates the fluctuation of Air Pressure in relation to time. The observation has shown a consistent decrease in the air pressure inside the initial cylinder (left) of O-HyPES with time. This may be attributed to the mixing of air with the contents of the Compressor Air storage (CAS). The observed phenomenon may be attributed to the increase in mass inside the Compressor Air storage (CAS). This is caused by a decrease in the mass of air within the first cylinder (left) of O-HyPES before to entering the CAS, leading to a subsequent fall in pressure.

Height of liquids' surfaces; Plot 2 **Figure 12** illustrates the alteration of the liquid's surface in both tanks when the air is compressed in relation to the datum. The rise in the height of the liquid's surface inside the left cylinder may be attributed to the compression exerted on the liquid by the pump during the charging mode, as previously discussed in the C-HyPES section. Conversely, there is a reduction in the level of the liquid's surface in the right cylinder, indicating that the fluid used in the process is of an incompressible nature.

Flow-rate; Plot 3 **Figure 12** illustrates the temporal fluctuations in flow-rate during the compression phase, particularly when the left valve is in an open state.

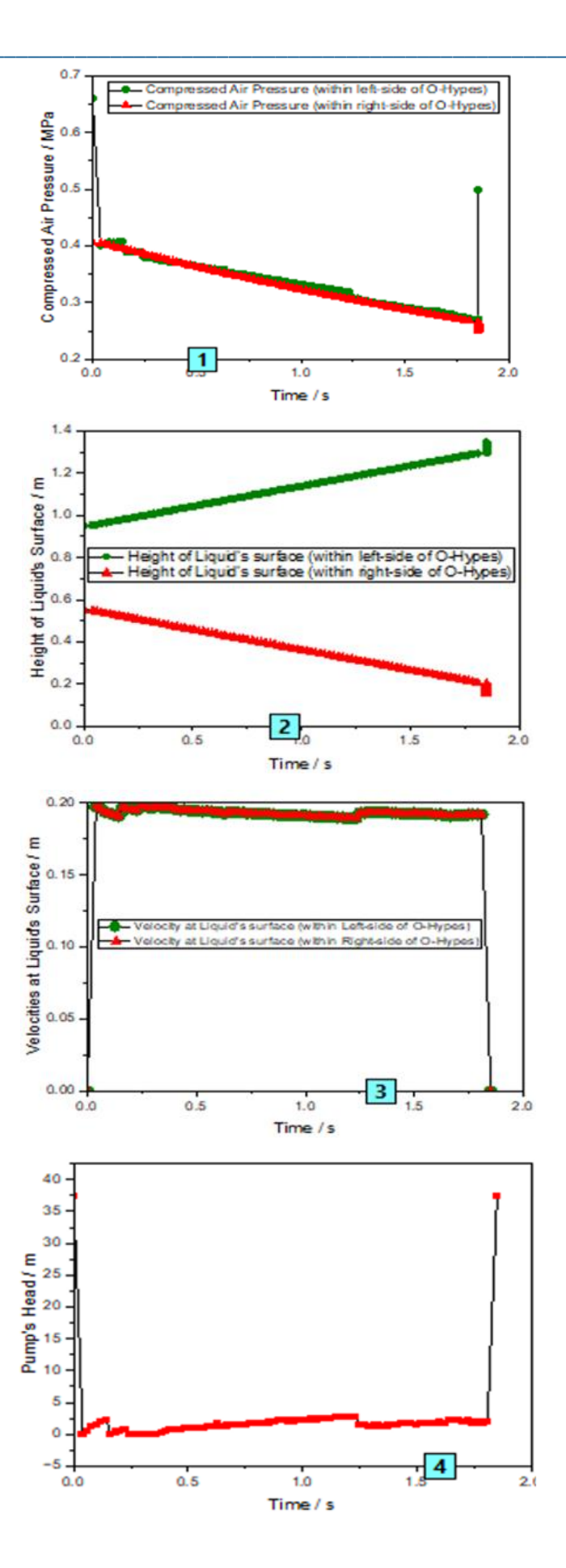
Velocity at liquids' Surfaces; Plot 4 **Figure 12,** there is a declining tendency seen in the flow rate with time. This may be attributed to a reduction in the pressure differential between the air in the first cylinder (left) of O-HyPES and the Compressed Air Storage system.

Pump's Head; Plot 5 **Figure 12** illustrates the fluctuation of the Pump's Head during the charging mode operation over time. In general, there is an upward trend in the head of the Pump over time. This indicates that the stored fluid inside the O-HyPES system has accumulated energy for the pump.

Pump's Efficiency; Plot 6 **Figure 12** depicts the graphical representation of the efficiency of the pump as a function of time. The data indicates that the efficiency of the pump remains rather stable over a duration of around 8 seconds.

Pump's Input power; Plot 7 **Figure 12** depicts how the Pump's input power changed over time. The fluctuation in the pump's input power has been noted to be rather minor across the time span between 0.8 seconds. This indicates that the head pump and its associated flow rate impacts on the efficiency of the pump do indeed work in opposition to one another.

Vol. 44 No. 6 (2023)



Vol. 44 No. 6 (2023)

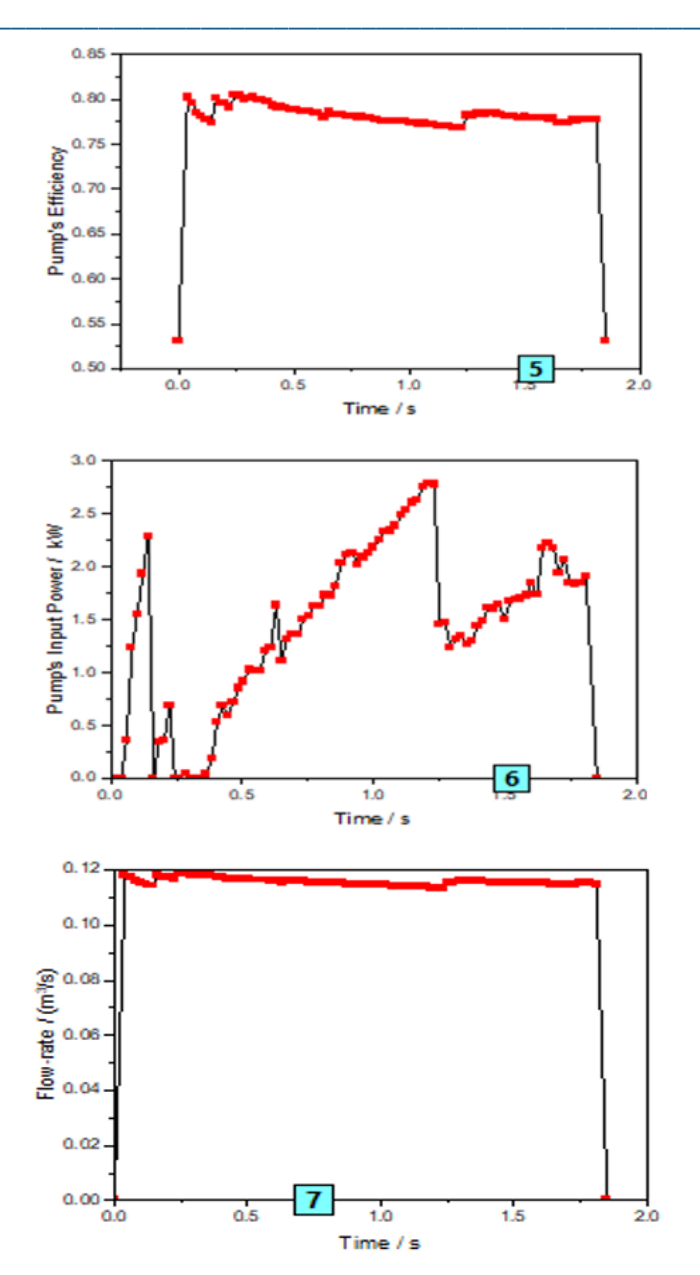


Figure 12. Shows 7 Plots of Resulted Variables of Stage-2 of O-HyPES

5.4. Resulted Variables of Stage 3

Pressure; Plot 1 Figure 13. represents the variation of the Air Pressure within the second cylinder (right of O-HyPES) with respect to the time throughout stage 3. It is observed that the pressure of the air increases over the range of time until it becomes constant at about 1.8 seconds.

Height of liquids' Surfaces; Plot 2 in Figure 13 shows the heights of the liquid surfaces tends to be constants with respect to the time throughout the stage 3.

Flow-rate; Plot 3 Figure 13 shows the variation of the flow-rate throughout stage 3 with respect to the time is displayed in Figure 92. The reasons for this behaviour are similar to that been mentioned within stage 1.

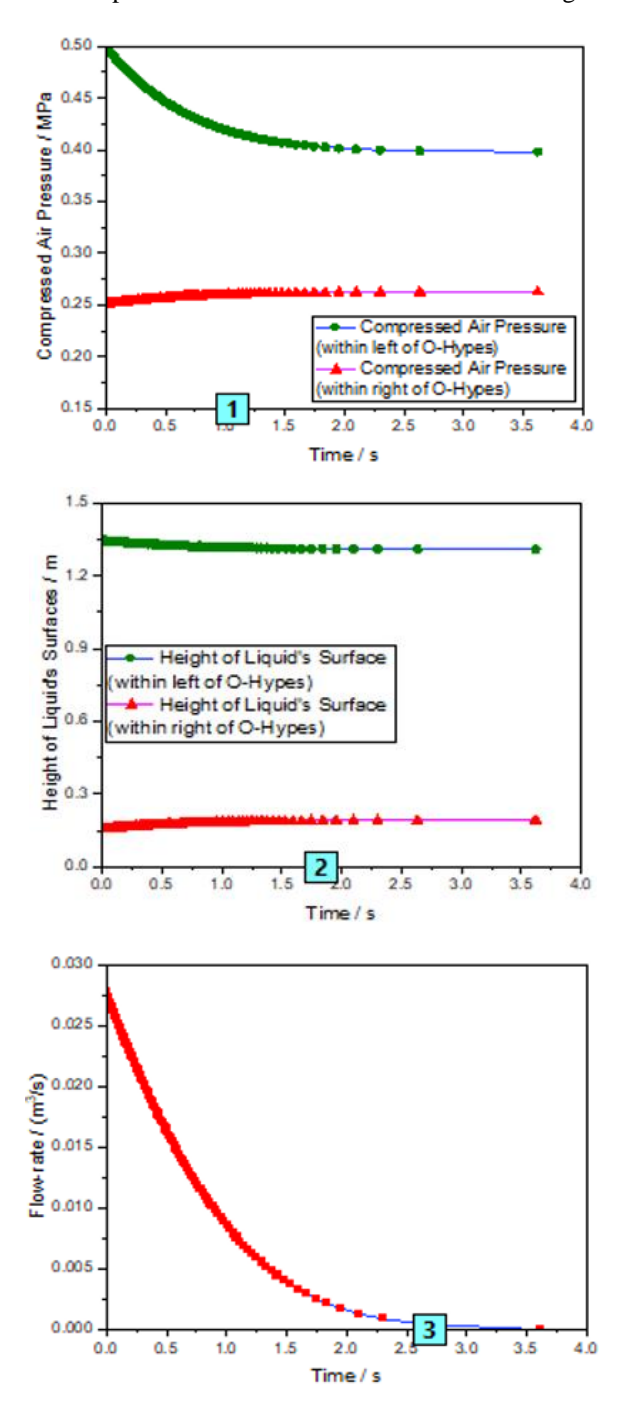
Velocity at liquids' Surfaces; Plot 4 in Figure 13 shows the reduction of velocity of the liquid surfaces due to the decline of the flow rate.

Turbine's Head; Plot 5 Figure 13 displays the graph of the Turbine's Head varies over time throughout stage 3. It is been remarked that the turbine's head is decreasing until it reaches to a minimum value, where its

corresponding time is about 0.25 seconds. After that, the head pump starts to rise where its gradient tends to be reduced with respect to the time.

Turbine's Output power; Plot 6 Figure 13 shows the variation of the turbine's output power over time. It is illustrated in the graph that equation (48) is not valid for the range of the time that lies between 0.06 and 0.8 seconds, as the obtained calculated values were found to be negative within this range of the time. Then the output power from the turbine would reach to its maximum value which occurs about the time of 1.0 seconds.

Turbine's Efficiency; Plot 7 Figure 13 shows the Turbine's Efficiency during the stage 3 in terms of the time. The increase of the Turbine's Efficiency has taken place for the range of time that is greater than 0.8 seconds, corresponding to the actual extracted power from the turbine has within this range of the time.



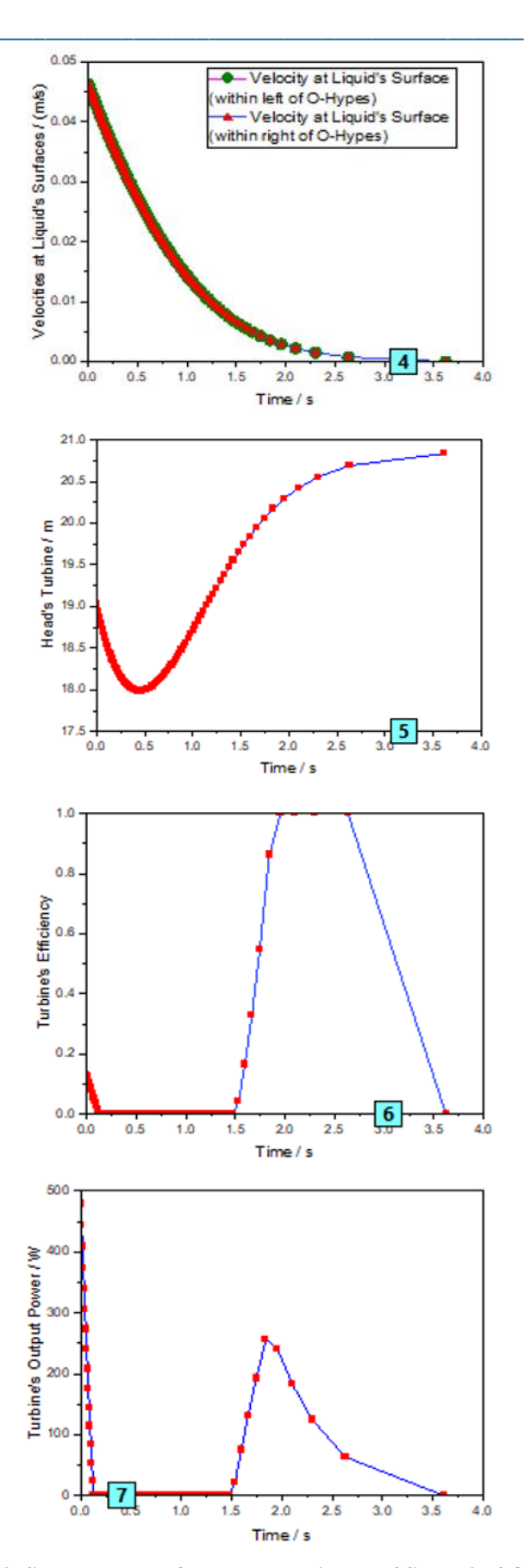


Figure 13. Shows 7 Plots of Resulted Variables of Stage-3 of O-HyPES

5.5. Resulted Variables of Stage 4

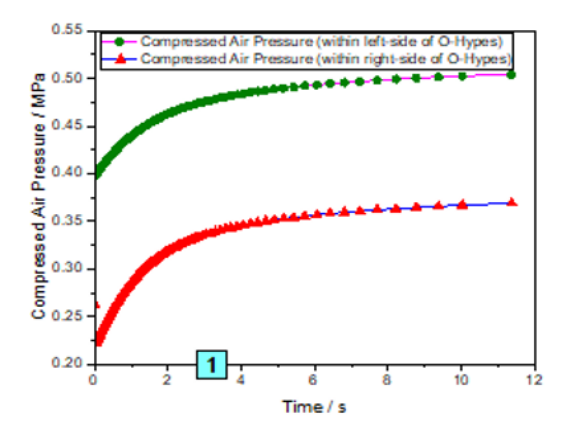
Pressure; Plot 1 **Figure 14** represents the graph of the Air Pressure within the second cylinder (right of O- HyPES) with respect to the time throughout stage 4, while the air from the right of O- HyPES is injected into Compressed Air Storage. Initially, it can be seen that the air pressure within the right of O- HyPES is increasing with respect to the time, where it would reach a point of inflexion at a time of 6 seconds, from which the gradient tends to get decreased till it reaches to constant value of about 3.7 MPa.

Flow-rate; Plot 3 **Figure 14** shows the variation of the flow-rate throughout stage 4 with respect to the time is displayed in. As the right valve is opened while the left valve is closed, the flow-rate of the flowing fluid tends to get increased till it reaches to its maximum value that occurs at a time of about 6 seconds with a value of 0.0027 m³/s. This can be attributed that the pressure difference between the air within the second cylinder (right) of O-HyPES and Compressed Air Storage has been increased throughout this time. As for the range of the time where the flow-rate tends to be decreasing over the time, it has been thought that the pressure difference Compressed Air Storage would have decreased throughout this time.

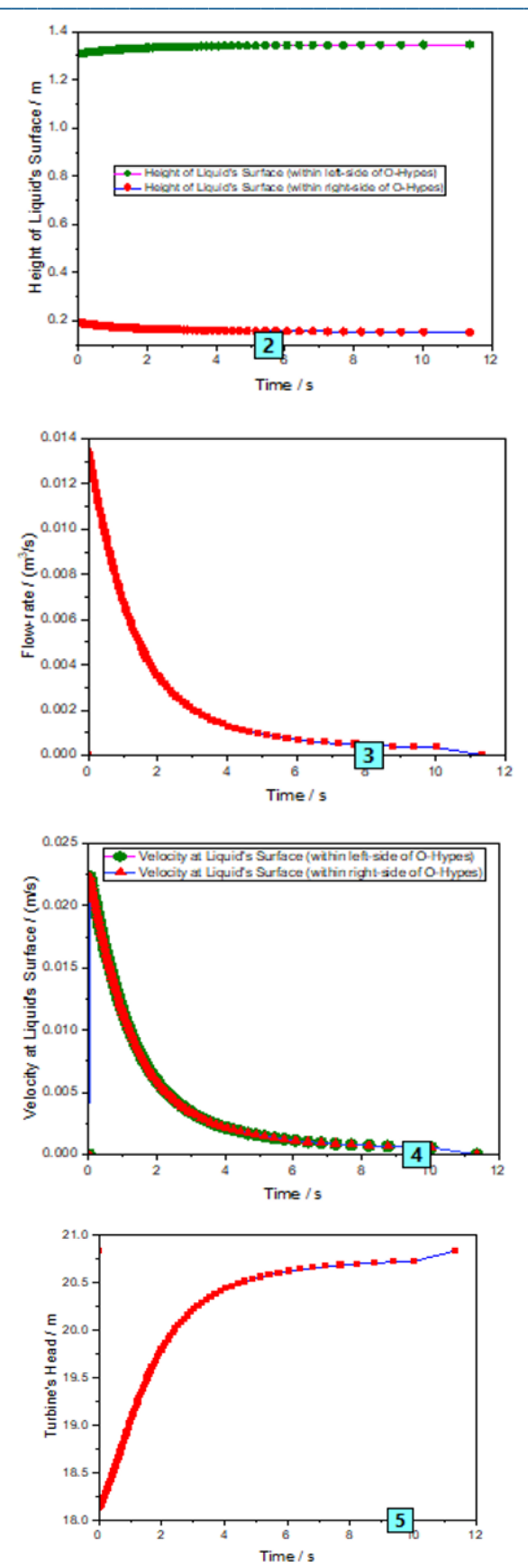
Turbine's Head; Plot 5 **Figure 14** represents the graph of the Turbine's Head varies over time throughout stage 4. It is been noticed that the turbine's head is decreasing until it reaches to its minimum value, corresponding to the time of about 6 seconds. Same reasons as been mentioned within the section of the flow-rate, where it is thought the rise of the pressure difference between the air within the second cylinder (right) of O- HyPES and Compressed Air Storage has taken place throughout this time. On the other-hand, the rise of the Turbine's Head for the time that is greater than 6 seconds, which can be interpreted that the decline of the pressure difference between the air within the second cylinder (right) of O- HyPES and Compressed Air Storage has taken place during this time.

Turbine's Output power; Plot 6 Figure 14 represents the graph of the Turbine's Output Power with respect to the time throughout stage 4. It is remarked that an increase in the Turbine's Output power has occurred over the range of the time that lies between 0 and 4.93 seconds as the obtained values of the hydraulic power (based on the flow-rate and turbine's head) are greater than the values of the power been obtained from equation (48) throughout this range. For the range of the time that takes place between 4.93 and 7.44 seconds, it was noticed that the values of the power been obtained based on equation (48) are greater than the values of their corresponding hydraulic power. For the range of the time that are greater than 7.44 seconds, it is attributed that the calculated hydraulic power values dominate than the values of the power been obtained from equation (48) during this period.

Turbine's Efficiency; Plot 7 **Figure 14** display the variation of the Turbine's Efficiency in terms of the time within stage 4. Similar reasons to that been mentioned for the Turbine's Output Power section, the calculated values of the hydraulic power overcome that the calculated values based on equation (48) occur within the ranges of times that are lower than 4.93 seconds and greater than 7.44 seconds. The range of the time where the calculated values of the power using equation (48) are greater than the determined values of the hydraulic power takes place between 4.93 and 7.44 seconds.







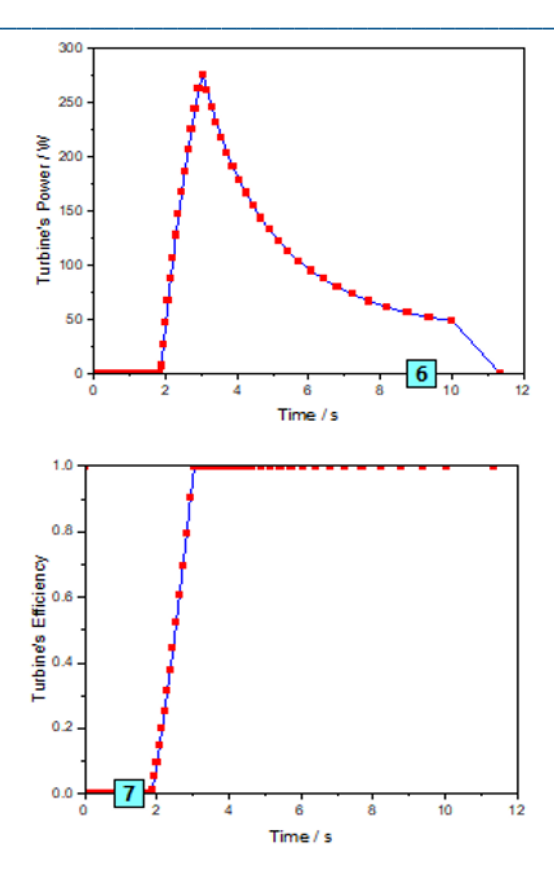


Figure 14. Shows 7 Plots of Resulted Variables of Stage-4 of O-HyPES

6. Head's Pump Impact on the Flow-rates at (BEP) for C-HyPES and O-HyPES

The following figure represents the variation of the flow-rates (BEP) with respect to the Head's Pump (BEP) for a given efficiency. It is observed that as the head's pump (BEP), it is corresponding the flow-rates (BEP) is decreased for a given efficiency. The following figure also displays that for the same range of the Head's Pump, the flow-rates (BEP) been obtained for the efficiency of 0.85 is higher compared to that been obtained for the efficiency of 0.8.

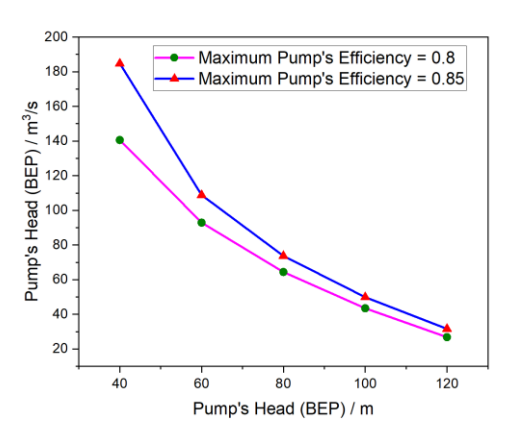


Figure 15. Flow-rate (BEP) vs Pump's Head (BEP) for different Efficiencies of the Pump.

7. Conclusions

The current study effectively introduced a novel correlation model for compressed air energy storage (CAES) that incorporates the utilisation of actual air properties. Furthermore, this study explored the thermodynamic properties relevant to isothermal processes, providing a comprehensive reference for both theoretical understanding and practical implementation of the subject matter. The suggested connections have contributed to the advancement

of knowledge about the basic thermodynamic concepts that form the basis of Compressed Air Energy Storage (CAES). This study additionally provided a theoretical foundation for comprehending the characteristics of Actual Air (AA), emphasising the essentiality of accurate fluid property information in the calculation and advancement of Compressed Air Energy Storage (CAES) methodologies. Moreover, this scholarly article presented a theoretical framework that facilitates the comprehension of the distinctive attributes of Actual Air (AA). The present research aims to examine the proposed associations between the physicochemical characteristics of air and the evaluation of the cycle efficiency of an isothermal process.

Authors Contribution

The main author of this research paper is Dr Mohamed Ammar who did the study from inception to completion. Additionally, has played a significant role in conceiving and designing the research, collecting and analysing data, interpreting results, and writing and revising the manuscript. Specifically, has: Collaboratively formulated the research objectives and hypotheses, made the data collection, either through experiments, surveys, or data acquisition, conducted statistical analyses and interpreted the findings jointly, the other authors contributed equally to the drafting and revision of the manuscript, including the literature review and discussion sections, and reviewed and approved the final version of the manuscript for submission. We affirm that all authors are in full agreement with the content of the manuscript.

Acknowledgement

The authors would kindly acknowledge the contribution of Innovate UK, the funding body of this work through Innovate UK Smart Grants project 10034102.

References

- [1] C. Qin, E. L.-A. Energy, and undefined 2014, "Liquid piston compression efficiency with droplet heat transfer," *Elsevier*, Accessed: Aug. 04, 2023. [Online]. Available: https://www.sciencedirect.com/science/article/pii/S0306261913008258
- [2] A. M. Rabi, J. Radulovic, and J. M. Buick, "Comprehensive Review of Compressed Air Energy Storage (CAES) Technologies," *Thermo 2023, Vol. 3, Pages 104-126*, vol. 3, no. 1, pp. 104–126, Jan. 2023, doi: 10.3390/THERMO3010008.
- [3] D. Wolf, M. B.-A. Energy, and undefined 2014, "LTA-CAES—a low-temperature approach to adiabatic compressed air energy storage," *Elsevier*, Accessed: Aug. 04, 2023. [Online]. Available: https://www.sciencedirect.com/science/article/pii/S0306261914002359
- [4] W. Liu *et al.*, "Analysis and optimization of a compressed air energy storage—combined cycle system," *mdpi.comW Liu, L Liu, L Zhou, J Huang, Y Zhang, G Xu, Y YangEntropy, 2014•mdpi.com*, vol. 16, pp. 3103–3120, 2014, doi: 10.3390/e16063103.
- [5] Y. Kim, D. F.- Energy, and undefined 2010, "Energy and exergy analysis of a micro-compressed air energy storage and air cycle heating and cooling system," *Elsevier*, Accessed: Aug. 04, 2023. [Online]. Available: https://www.sciencedirect.com/science/article/pii/S0360544209003971
- [6] Z. Yang, Z. Wang, P. Ran, Z. Li, W. N.-A. thermal engineering, and undefined 2014, "Thermodynamic analysis of a hybrid thermal-compressed air energy storage system for the integration of wind power," *Elsevier*, Accessed: Aug. 04, 2023. [Online]. Available: https://www.sciencedirect.com/science/article/pii/S1359431114001355
- [7] A. B. Ennil, "Optimization of small-scale axial turbine for distributed compressed air energy storage system," 2017, Accessed: Aug. 04, 2023. [Online]. Available: https://etheses.bham.ac.uk/id/eprint/7157/
- [8] P. Zhao, L. Gao, J. Wang, Y. D.-R. Energy, and undefined 2016, "Energy efficiency analysis and off-design analysis of two different discharge modes for compressed air energy storage system using axial turbines," *Elsevier*, Accessed: Aug. 04, 2023. [Online]. Available: https://www.sciencedirect.com/science/article/pii/S0960148115301907
- [9] J. Wojcik, J. W.-A. Energy, and undefined 2018, "Feasibility study of combined cycle gas turbine (CCGT) power plant integration with adiabatic compressed air energy storage (ACAES)," *Elsevier*, Accessed: Aug. 04, 2023. [Online]. Available: https://www.sciencedirect.com/science/article/pii/S0306261918304288

- [10] Y. Kim, J. Lee, S. Kim, D. F.- Entropy, and undefined 2012, "Potential and evolution of compressed air energy storage: energy and exergy analyses," *mdpi.comYM Kim, JH Lee, SJ Kim, D FavratEntropy, 2012•mdpi.com*, vol. 14, pp. 1501–1521, 2012, doi: 10.3390/e14081501.
- [11] C. Knowlen, J. Williams, A. T. Mattick, H. Deparis, and A. Hertzberg, "Quasi-Isothermal Expansion Engines for Liquid Nitrogen Automotive Propulsion," *SAE Technical Papers*, Aug. 1997, doi: 10.4271/972649.
- [12] X. Luo *et al.*, "Modelling study, efficiency analysis and optimisation of large-scale Adiabatic Compressed Air Energy Storage systems with low-temperature thermal storage," *Elsevier*, Accessed: Aug. 04, 2023. [Online]. Available: https://www.sciencedirect.com/science/article/pii/S0306261915013185
- [13] N. Hartmann, O. Vöhringer, C. Kruck, L. E.-A. energy, and undefined 2012, "Simulation and analysis of different adiabatic compressed air energy storage plant configurations," *Elsevier*, Accessed: Aug. 04, 2023. [Online]. Available: https://www.sciencedirect.com/science/article/pii/S0306261911008014
- [14] L. Geissbühler, V. Becattini, ... G. Z.-J. of E., and undefined 2018, "Pilot-scale demonstration of advanced adiabatic compressed air energy storage, Part 1: Plant description and tests with sensible thermal-energy storage," *Elsevier*, Accessed: Aug. 04, 2023. [Online]. Available: https://www.sciencedirect.com/science/article/pii/S2352152X17305546
- [15] L. Geissbühler, V. Becattini, ... G. Z.-J. of E., and undefined 2018, "Pilot-scale demonstration of advanced adiabatic compressed air energy storage, Part 1: Plant description and tests with sensible thermal-energy storage," *Elsevier*, Accessed: Aug. 04, 2023. [Online]. Available: https://www.sciencedirect.com/science/article/pii/S2352152X17305546
- [16] S. Wang, X. Zhang, L. Yang, Y. Zhou, J. W.- Energy, and undefined 2016, "Experimental study of compressed air energy storage system with thermal energy storage," *Elsevier*, Accessed: Aug. 04, 2023. [Online]. Available: https://www.sciencedirect.com/science/article/pii/S0360544216301876
- [17] X.-K. Wen *et al.*, "Compressed Air Energy Storage and Future Development," *iopscience.iop.orgJ Guo*, *R Ma*, *H ZouJournal of Physics: Conference Series*, 2021•iopscience.iop.org, vol. 2108, p. 12037, 2021, doi: 10.1088/1742-6596/2108/1/012037.
- [18] S. Alirahmi, S. Mousavi, ... A. R.-E. C. and, and undefined 2021, "A comprehensive techno-economic analysis and multi-criteria optimization of a compressed air energy storage (CAES) hybridized with solar and desalination," *Elsevier*, Accessed: Aug. 04, 2023. [Online]. Available: https://www.sciencedirect.com/science/article/pii/S0196890421002296
- [19] A. Razmi, H. Afshar, ... A. P.-... E. T. and, and undefined 2021, "Investigation of a combined heat and power (CHP) system based on biomass and compressed air energy storage (CAES)," *Elsevier*, Accessed: Aug. 04, 2023. [Online]. Available: https://www.sciencedirect.com/science/article/pii/S2213138821002630
- [20] G. Venkataramani, P. Vijayamithran, Y. Li, Y. D.- Energy, and undefined 2019, "Thermodynamic analysis on compressed air energy storage augmenting power/polygeneration for roundtrip efficiency enhancement," *Elsevier*, Accessed: Aug. 04, 2023. [Online]. Available: https://www.sciencedirect.com/science/article/pii/S0360544219309016
- [21] N. Hartmann, O. Vöhringer, C. Kruck, L. E.-A. energy, and undefined 2012, "Simulation and analysis of different adiabatic compressed air energy storage plant configurations," *Elsevier*, Accessed: Aug. 04, 2023. [Online]. Available: https://www.sciencedirect.com/science/article/pii/S0306261911008014
- [22] D. Wolf, M. B.-A. Energy, and undefined 2014, "LTA-CAES—a low-temperature approach to adiabatic compressed air energy storage," *Elsevier*, Accessed: Aug. 04, 2023. [Online]. Available: https://www.sciencedirect.com/science/article/pii/S0306261914002359
- [23] K. Yang, Y. Zhang, X. Li, J. X.-E. conversion and management, and undefined 2014, "Theoretical evaluation on the impact of heat exchanger in advanced adiabatic compressed air energy storage system," *Elsevier*, Accessed: Aug. 04, 2023. [Online]. Available: https://www.sciencedirect.com/science/article/pii/S0196890414005871
- [24] Y. Li *et al.*, "A reserve capacity model of AA-CAES for power system optimal joint energy and reserve scheduling," *Elsevier*, Accessed: Aug. 04, 2023. [Online]. Available: https://www.sciencedirect.com/science/article/pii/S0142061518309992

[25] X. Luo et al., "Modelling study, efficiency analysis and optimisation of large-scale Adiabatic Compressed Air Energy Storage systems with low-temperature thermal storage," Elsevier, Accessed: Aug. 04, 2023.

- [Online]. Available: https://www.sciencedirect.com/science/article/pii/S0306261915013185 [26] A. Sciacovelli *et al.*, "Dynamic simulation of Adiabatic Compressed Air Energy Storage (A-CAES) plant with integrated thermal storage—Link between components performance," *Elsevier*, Accessed: Aug. 04, 2023. [Online]. Available: https://www.sciencedirect.com/science/article/pii/S0306261916315021
- [27] S. Succar, R. W.-P. environmental institute report, and undefined 2008, "Compressed air energy storage: theory, resources, and applications for wind power," *CiteseerS Succar, RH WilliamsPrinceton environmental institute report, 2008•Citeseer*, Accessed: Aug. 04, 2023. [Online]. Available: https://citeseerx.ist.psu.edu/document?repid=rep1&type=pdf&doi=07b1c66eba1504846d7b49bc4fffc5725a17e57e
- [28] "Geng, X.; Zhu, Q.; Guo, H.; Duan, C.; Cui, H. Energy... Google Scholar."
- [29] B. Zakeri, S. S.-R. and sustainable energy reviews, and undefined 2015, "Electrical energy storage systems: A comparative life cycle cost analysis," *Elsevier*, Accessed: Aug. 04, 2023. [Online]. Available: https://www.sciencedirect.com/science/article/pii/S1364032114008284
- [30] L. Li, W. Liang, H. Lian, J. Yang, and M. Dusseault, "Compressed air energy storage: Characteristics, basic principles, and geological considerations," *Advances in Geo-Energy Research*, vol. 2, no. 2, pp. 135–147, Jun. 2018, doi: 10.26804/AGER.2018.02.03.
- [31] S. Hameer, J. van N.-I. journal of energy, and undefined 2015, "A review of large-scale electrical energy storage," *Wiley Online LibraryS Hameer, JL van NiekerkInternational journal of energy research, 2015•Wiley Online Library*, vol. 39, no. 9, pp. 1179–1195, Jul. 2015, doi: 10.1002/er.3294.
- [32] "Luo, X.; Wang, J.; Ma, Z. Overview of energy storage... Google Scholar."
- [33] G. Venkataramani, ... P. P.-... and sustainable energy, and undefined 2016, "A review on compressed air energy storage—A pathway for smart grid and polygeneration," *Elsevier*, Accessed: Aug. 04, 2023. [Online]. Available: https://www.sciencedirect.com/science/article/pii/S1364032116301125
- [34] T. Mahlia, T. Saktisahdan, ... A. J.-... and sustainable energy, and undefined 2014, "A review of available methods and development on energy storage; technology update," *Elsevier*, Accessed: Aug. 04, 2023. [Online]. Available: https://www.sciencedirect.com/science/article/pii/S1364032114000902
- [35] T. Kousksou, P. Bruel, A. Jamil, ... T. E. R.-S. E. M., and undefined 2014, "Energy storage: Applications and challenges," *Elsevier*, Accessed: Aug. 04, 2023. [Online]. Available: https://www.sciencedirect.com/science/article/pii/S0927024813004145
- [36] Y. Zhang, Y. Xu, X. Zhou, H. Guo, X. Zhang, and H. Chen, "Compressed air energy storage system with variable configuration for wind power generation," *Energy Procedia*, vol. 142, pp. 3356–3362, Dec. 2017, doi: 10.1016/J.EGYPRO.2017.12.470.
- [37] J. Chen *et al.*, "Preliminary investigation on the feasibility of a clean CAES system coupled with wind and solar energy in China," *Energy*, vol. 127, pp. 462–478, May 2017, doi: 10.1016/J.ENERGY.2017.03.088.
- [38] W. Ji, Y. Zhou, Y. Sun, W. Zhang, B. An, and J. Wang, "Thermodynamic analysis of a novel hybrid wind-solar-compressed air energy storage system," *Energy Convers Manag*, vol. 142, pp. 176–187, Jun. 2017, doi: 10.1016/J.ENCONMAN.2017.02.053.
- [39] J. Fan *et al.*, "Thermodynamic and applicability analysis of a hybrid CAES system using abandoned coal mine in China," *Energy*, vol. 157, pp. 31–44, Aug. 2018, doi: 10.1016/J.ENERGY.2018.05.107.
- [40] Z. Han, S. Guo, S. Wang, and W. Li, "Thermodynamic analyses and multi-objective optimization of operation mode of advanced adiabatic compressed air energy storage system," *Energy Convers Manag*, vol. 174, pp. 45–53, Oct. 2018, doi: 10.1016/J.ENCONMAN.2018.08.030.
- [41] Y. Yan, C. Zhang, K. Li, C. Tian, and F. Wang, "An Active Control Strategy for Composited Energy Storage with Compressed Air Energy Storage in Micro-Grid," *Diangong Jishu Xuebao/Transactions of China Electrotechnical Society*, vol. 32, no. 20, pp. 231–240, Oct. 2017, doi: 10.19595/J.CNKI.1000-6753.TCES.160628.
- [42] Y. Yan, C. Zhang, K. Li, and Z. Wang, "An integrated design for hybrid combined cooling, heating and power system with compressed air energy storage," *Appl Energy*, vol. 210, pp. 1151–1166, Jan. 2018, doi: 10.1016/J.APENERGY.2017.07.005.

[43] J. Fan *et al.*, "Thermodynamic and applicability analysis of a hybrid CAES system using abandoned coal mine in China," *Energy*, vol. 157, pp. 31–44, Aug. 2018, doi: 10.1016/J.ENERGY.2018.05.107.

- [44] Z. Han and S. Guo, "Investigation of discharge characteristics of a tri-generative system based on advanced adiabatic compressed air energy storage," *Energy Convers Manag*, vol. 176, pp. 110–122, Nov. 2018, doi: 10.1016/J.ENCONMAN.2018.09.026.
- [45] H. Guo, Y. Xu, H. Chen, C. Guo, and W. Qin, "Thermodynamic analytical solution and exergy analysis for supercritical compressed air energy storage system," *Appl Energy*, vol. 199, pp. 96–106, Aug. 2017, doi: 10.1016/J.APENERGY.2017.04.068.
- [46] Z. Tong, Z. Cheng, S. T.-R. and S. E. Reviews, and undefined 2021, "A review on the development of compressed air energy storage in China: Technical and economic challenges to commercialization," *Elsevier*, Accessed: Aug. 04, 2023. [Online]. Available: https://www.sciencedirect.com/science/article/pii/S136403212030469X
- [47] I. Glendenning, P. E. Chew, R. Grant, R. Glanville, and M. H. Moye, "Technical and economic assessment of advanced compressed air storage (ACAS) concepts. Final report." 1979.
- [48] M. Budt, D. Wolf, R. Span, J. Y.-A. energy, and undefined 2016, "A review on compressed air energy storage: Basic principles, past milestones and recent developments," *Elsevier*, Accessed: Jul. 18, 2023. [Online]. Available: https://www.sciencedirect.com/science/article/pii/S0306261916302641
- [49] S. Freund, R. Schainker, and R. Moreau, "Commercial concepts for adiabatic compressed air energy storage," 2012, Accessed: Jul. 18, 2023. [Online]. Available: https://www.osti.gov/etdeweb/biblio/22119356
- [50] H. Chen, T. N. Cong, W. Yang, C. Tan, Y. Li, and Y. Ding, "Progress in electrical energy storage system: A critical review," *Progress in Natural Science*, vol. 19, no. 3, pp. 291–312, Mar. 2009, doi: 10.1016/J.PNSC.2008.07.014.
- [51] L. W. M. Beurskens, M. De Noord, and A. F. Wals, "Analysis in the framework of the INVESTIRE network. Economic performance of storage technologies." 2003.
- [52] S. Succar, R. W.-P. environmental institute report, and undefined 2008, "Compressed air energy storage: theory, resources, and applications for wind power," *Citeseer*, Accessed: Jul. 21, 2023
- [53] "Huntorf 290 MW the world's first Air Storage System Energy Transfer (ASSET) plant: construction and commissioning (Conference) | OSTI.GOV." https://www.osti.gov/biblio/5853061 (accessed Jul. 18, 2023).
- [54] A. M. Rabi, J. Radulovic, and J. M. Buick, "Comprehensive Review of Compressed Air Energy Storage (CAES) Technologies," *Thermo 2023, Vol. 3, Pages 104-126*, vol. 3, no. 1, pp. 104–126, Jan. 2023, doi: 10.3390/THERMO3010008.
- [55] M. King, A. Jain, R. Bhakar, J. Mathur, and J. Wang, "Overview of current compressed air energy storage projects and analysis of the potential underground storage capacity in India and the UK," *Renewable and Sustainable Energy Reviews*, vol. 139, p. 110705, Apr. 2021, doi: 10.1016/J.RSER.2021.110705.
- [56] A. S. Alsagri, A. Arabkoohsar, and A. A. Alrobaian, "Combination of subcooled compressed air energy storage system with an Organic Rankine Cycle for better electricity efficiency, a thermodynamic analysis," *J Clean Prod*, vol. 239, p. 118119, Dec. 2019, doi: 10.1016/J.JCLEPRO.2019.118119.
- [57] H. Mozayeni, "Development of a Combined Pumped Hydro and Compressed Air Energy Storage System," 2019, doi: 10.1016/j.scs.2019.101527.
- [58] Q. Yu, X. Li, Y. Geng, and X. Tan, "Study on quasi-isothermal expansion process of compressed air based on spray heat transfer," *Energy Reports*, vol. 8, pp. 1995–2007, Nov. 2022, doi: 10.1016/j.egyr.2022.01.019.
- [59] S. Succar and R. H. Williams, "NRC Staff Prefiled Hearing Exhibit NRC000040, Samir Succar & Robert H. Williams, Princeton University: Energy Systems Analysis Group, Compressed Air Energy Storage: Theory, Resources, and Applications for Wind Power (2008)."